Geomechanics and Engineering, *Vol. 41, No. 5 (2025) 493-505*
https://doi.org/10.12989/gae.2025.41.5.493

Experimental evidences on a unique critical state line for coarse-grained soil with different gradations in light of skeleton void ratio

Feng Gao[1a], Jungao Zhu*[1], Tao Wang[2b], Qixun Luo[3c], Xiaoan Wang[3d] and Lei Pan[4e]

[1]*Key Laboratory of Ministry of Education for Geomechanics and Embankment Engineering, Hohai University, 01 Xikang Road, Nanjing 210098, China*
[2]*School of Earth Sciences and Engineering, Nanjing University, 163 Xianlin Road, Nanjing 210023, China*
[3]*Chengdu Engineering Corporation Limited, Power China. Chengdu, Sichuan 610072, China*
[4]*Shanghai research institute of building sciences co..Ltd. Shanghai 200032, China*

(*Received January 1, 2025, Revised March 10, 2025, Accepted May 9, 2025*)

Abstract. In the e-(p'/p_a) plane, the critical state line (CSL) under different gradations exhibits translation and rotation, which increases the uncertainty of the state parameter. The constitutive model based on the state parameter faces challenges in predicting whether coarse-grained soil will exhibit dilatancy or contraction. The selection of the void ratio index is one of the important factors. This study conducts large-scale triaxial compression tests under different gradations, introduces the concept of skeleton void ratio, and compares the effect of gradation on CSL. The results show that the initial gradation significantly affects the critical void ratio of coarse-grained soils but has little effect on the critical stress ratio. Different gradations cause the CSL in the e-(p'/p_a) plane to translation and rotate, whereas in the e_{sk}-(p'/p_a) plane, the CSL converges to a single curve. A linear relationship exists between the parameter b of the skeleton void ratio and the fractal dimension D, and the parameters α = 0.13 and β = -1.5 are applicable to most coarse-grained soils. This finding will simplify the application of the skeleton void ratio. The unified CSL equation proposed in this study provides a good foundation for developing state-dependent constitutive models.

Keywords: coarse-grained soil; CSL; gradation; skeleton void ratio; triaxial test

1. Introduction

Coarse-grained soil, widely used as primary construction materials for structures such as earth-rockfill dam (Baak *et al*. 2017, Wu *et al*. 2024) and railway ballast (Kian *et al*. 2018, Abadi *et al*. 2023), play a crucial role in geotechnical engineering. Under shear deformation, coarse-grained soil eventually reaches a critical state where the mean effective stress, deviatoric stress, and volumetric strain stabilize, while shear strain continues to evolve (Fonseca *et al*. 2023). This critical state, as a stable reference condition, serves as a benchmark for comparing the current state of the soil to assess whether it is in a dense or loose state and to predict whether dilatancy or contraction is likely to occur (Ning *et al*. 2020). Such insights are vital for the development of state-dependent dilatancy equations and constitutive models (Sun *et al*. 2019, Ng *et al*. 2024).

Gradation is one of the most critical factors influencing the behavior of soil (Jiang *et al*. 2018, Ahmed *et al*. 2023, Shi *et al*. 2024, Shi *et al*. 2025). Coarse-grained soils with different gradations, even under the same confining pressure, reach different critical states, resulting in distinct critical state lines (CSLs) (Xiao *et al*. 2016, Guo *et al*. 2024). Specifically, as the gradation becomes broader, the CSL in the e-$(p'/p_a)^{\xi}$ plane shifts downward and rotates, where e is the global void ratio, p' denotes the mean effective pressure, p_a represents the atmospheric pressure and ξ is a material constant (Muir Wood and Maeda 2008, Yan and Dong 2011). The variation in CSLs under different gradations indicates that it is difficult to accurately obtain the critical state parameters of the material when developing state-dependent constitutive models. This significantly complicates the process of incorporating the gradation effect into state-dependent constitutive models for coarse-grained soil.

The translation and rotation of the CSL are closely related to the method used to measure void ratio. In recent years, some researchers (Dash and Sitharam 2011, Dai *et al*. 2019) have suggested that global void ratio lack precision. They propose that fine particles within the soil skeleton, which do not contribute to stress transmission, act as voids and should be considered part of the void volume when calculating void ratio (Yin *et al*. 2014, Chang *et al*. 2015, Zamani and Montoya 2018). This perspective led to the definition and calculation of the skeleton void ratio e_{sk}, which has been applied in studies of sand-silt mixtures, such as small-strain dynamic behavior (Payan *et al*. 2017a, Payan and Senetakis 2018, Payan *et al*. 2020, Khodkari *et al*. 2024). When the skeleton void ratio replaces the global void ratio, the CSLs of sand-silt mixtures with different

*Corresponding author, Professor
E-mail: zhujungao@hhu.edu.com
[a]Ph.D. Student
[b]Ph.D.
[c]Senior Engineer
[d]Senior Engineer
[e]Ph.D.

Copyright © 2025 Techno-Press, Ltd.

ISSN: 2005-307X (Print), 2092-6219 (Online)


(a) Large-scale triaxial apparatus


(b) Sample preparation

Fig. 1 Large-scale triaxial compression test

gradations converge into a narrow band. This implies that sand-silt mixtures with varying gradations approximately share a unified CSL (Yang *et al*. 2006, Chang and Yin 2011). This finding is significant for developing state-dependent constitutive models that account for gradation effects. However, it remains unclear whether this conclusion is applicable to wide-graded coarse-grained soils. Therefore, there is an urgent need for experimental evidences to validate whether a unique CSL exists for coarse-grained soils with different gradations when using the skeleton void ratio. This is crucial for establishing a theoretical foundation for developing state-dependent constitutive models for coarse-grained soils that account for gradation effects.

This study addresses these gaps by: (1) conducting large-scale triaxial compression tests on coarse-grained soil to analyze the effects of confining pressure and initial gradation on their critical state behavior; (2) reviewing the theoretical foundation of the skeleton void ratio, leading to the development of a unified CSL equation based on the skeleton void ratio, which was validated using large-scale triaxial test data from existing literature; (3) exploring the relationship between the skeleton void ratio parameter b and the fractal dimension D, resulting in a linear relationship that links parameter b to the fractal dimension.

2. Test program

2.1 Apparatus and materials

The experimental apparatus used is the large-scale triaxial compression test at Hohai University, China, which can conduct triaxial tests on samples with a diameter of 300 mm and a height of 600 mm. As shown in Fig. 1, the instrument consists of several components, including the axial loading frame, pressure chamber, axial force loading device, confining pressure loading device, and computer control system. The maximum confining pressure that the instrument can withstand is 4 MPa, with a maximum axial load of 1000 kN and a maximum axial displacement of 125 mm, which corresponds to an axial strain of 21% in the sample. The volumetric change pipe has a capacity of 4000 ml and a resolution of 5 ml. In terms of axial load control, the deformation speed range of the instrument is 0.5 to 3.0 mm/min.

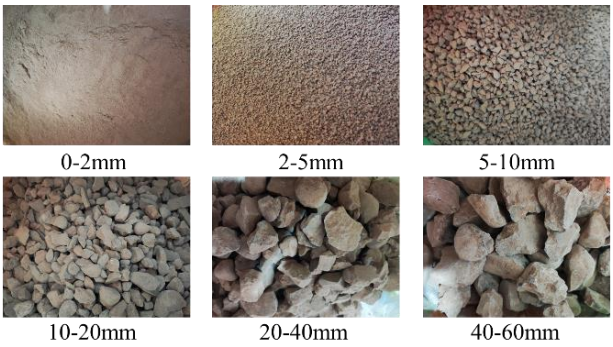

Fig. 2 Coarse-grained soils with different particle diameters

Table 1 Large-scale triaxial compression test scheme

Group	D_0	C_u	C_c	e_0	σ_3 (kPa)
G1	2.095	7.24	1.57	0.337	400/800/1600/3200
G2	2.352	15.88	1.87	0.300	400/800/1600/3200
G3	2.483	32.00	2.19	0.273	400/800/1600/3200
G4	2.561	59.23	2.52	0.259	400/800/1600/3200

Note: D_0 is initial fractal dimension, C_u is coefficient of uniformity, C_c is coefficient of curvature

The coarse-grained soils used in this study were sourced from a rockfill dam project in southwestern China, with a specific gravity G_s of 2.71. The diameter of a tested sample is 300 mm, with a maximum allowable particle size of 60 mm. Before the experiment, the coarse-grained soils were sieved into six particle groups, ranging from small to large: 0-2 mm, 2-5 mm, 5-10 mm, 10-20 mm, 20-40 mm, and 40-60 mm. The particle entities of each sieve size are shown in Fig. 2.

2.2 Tested gradations

To study the effect of gradation on the CSL, four different gradation groups were designed for the large-scale triaxial compression test. Each group of samples was subjected to shear under four confining pressures: 0.4 MPa, 0.8 MPa, 1.6 MPa, and 3.2 MPa, resulting in a total of 16 large triaxial samples. The layered compaction method was used for sample preparation, with each layer having a height of 120 mm, totaling five layers for an overall sample height of 600 mm. During the preparation process, the relative density of the sample was carefully controlled at 0.75 by ensuring uniform compaction for each layer. The specific experimental program and initial void ratio (dry density) is shown in Table 1, where groups G1 to G4 represent the four different gradations. The initial gradations are quantified by following fractal distributions and can be expressed as

$$P = \left(\frac{d}{d_{\max}} \right)^{3-D} \tag{1}$$

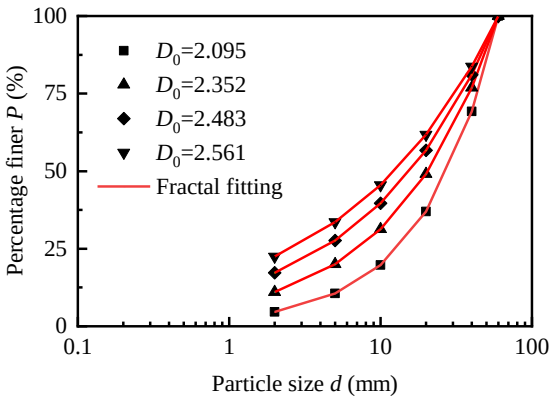

Fig. 3 Initial gradations of coarse-grained soils

Where P represents percentage finer, d is particle diameter, d_{max} is the maximum diameter, and D denotes fractal dimension.

Fig. 3 shows the particle size distribution of different initial gradations. According to the ASTM standard (ASTM 2006), a gradation with $C_u > 4$ and $1 < C_c < 3$ is classified as well-graded. All of the four designed gradations are well-graded.

3. Test results and analyses

3.1 Effect of confining pressure

To reflect the effects of confining pressure on the strength and deformation behavior of coarse-grained soils, the stress-strain relationships of samples with the same gradation but different confining pressures are plotted in Fig. 4. It can be found that in the early stages of the test, the increase in deviatoric stress is rapid, but after a certain point in the test, even as the axial strain continues to increase, the growth rate of deviatoric stress significantly slows down, eventually reaching a stable value. This stable value is referred to as the critical deviatoric stress q_c. Critical deviatoric stress is found to increases with increasing confining pressure. As for volumetric strain, the sample generally exhibits dilatancy under low confining pressures, whereas under high confining pressures, contraction is more likely to occur.

In addition, as axial strain develops, the initial gradients of deviatoric stress and volumetric strain both increase. For example, in Fig. 4(a), as the confining pressure increases from 400 kPa to 3200 kPa, the initial gradient of deviatoric stress increases from 692 kPa/% to 3046 kPa/%, and the initial gradient of volumetric strain increases from 0.53 to 1.02. This trend indicates that higher confining pressure enhances stiffness and suppresses dilatancy.

3.2 Effect of gradation

The stress-strain relationship curves for different particle gradations under the same confining pressure are shown in Fig. 5. It can be seen that under low confining pressure, the sample generally undergoes softening. For the samples under high confining pressure, hardening occurs when the fractal dimension is small, while softening occurs at large fractal dimension. Eventually, the deviatoric stress gradually stabilizes and approaches the critical state.

For the same axial strain, the deviatoric stress increases with the fractal dimension. When the fractal dimension is smaller, the axial strain required to reach the peak deviatoric stress is larger. This is because samples with a smaller fractal dimension contain more coarse particles, which break under compression, generating more fine particles that fill the pores, thus requiring greater axial strain to reach the peak deviatoric stress. This also implies that a larger axial strain is needed to reach the critical state. The initial gradient of deviatoric stress increases with the fractal dimension. For example, at a confining pressure of 1600 kPa, the initial gradient of deviatoric stress increases from 1583 kPa/% to 2290 kPa/%. This implies that finer gradation makes the sample denser and enhances its stiffness.

Moreover, as the fractal dimension increases, the volumetric strain of the sample shows a decreasing trend. For example, under a confining pressure of 1600 kPa, when the fractal dimension is 2.095, the maximum volumetric strain of the sample is 3.45%. However, when the fractal dimension increases to 2.561, the maximum volumetric strain decreases to 2.30%, accompanied by a more pronounced dilatancy phenomenon. This can be attributed to the increase in fractal dimension, which makes the sample denser and more prone to dilatancy. It can also be observed that a smaller fractal dimension corresponds to a larger axial strain at the dilatancy phase transition point. This occurs because a smaller fractal dimension indicates a higher proportion of coarse particles in the sample, which are more prone to breakage during the test. The resulting increase in fine particles necessitates particle rearrangement to achieve a stable state, prolonging the process. Additionally, the initial gradient of volumetric strain decreases with the fractal dimension. At a confining pressure of 1600 kPa, the initial gradient of volumetric strain decreases from 0.84 to 0.62. This implies that finer gradation makes the sample exhibit higher dilatancy.

4. CSLs in q-p' and e-$(p'/p_a)^{\xi}$ planes

4.1 CSL in the q-p′ plane

The deviatoric stress q and mean effective stress p' under different initial fractal dimension conditions are plotted in the q-p' plane, with the stress path following the conventional triaxial compression path, as shown in Fig. 6. It can be observed that, under high confining pressure, when the initial fractal dimension is small, the deviatoric stress increases gradually with the mean effective stress until it reaches the critical state deviatoric stress. However, when the initial fractal dimension is large, the deviatoric stress increases with the mean effective stress, reaches a peak value, and then decreases gradually to the critical deviatoric stress.

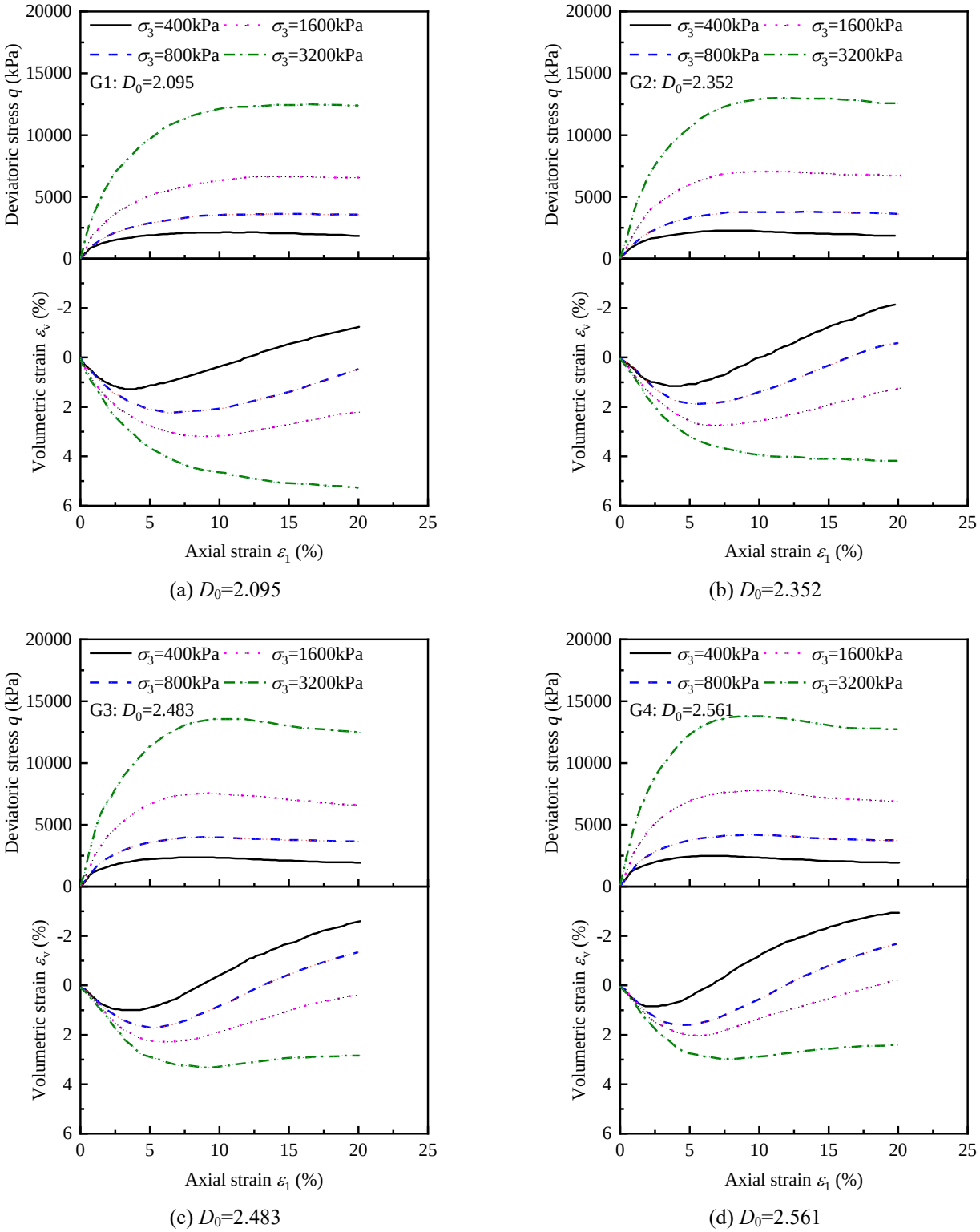

(a) D_0=2.095 (b) D_0=2.352

(c) D_0=2.483 (d) D_0=2.561

Fig. 4 Evolutions of deviatoric stress and volumetric strain with axial strain under different confining pressures

Under low confining pressure, regardless of the initial fractal dimension, the deviatoric stress consistently increases with the mean effective stress, reaches a peak, and then decreases to the critical state deviatoric stress. This behavior is mainly due to insufficient confining pressure to suppress dilatancy, which results in the formation of localized shear bands and a reduction in peak strength, exhibiting a softening phenomenon.

The critical state points under different initial gradations at various confining pressures are plotted in the q-p' plane,

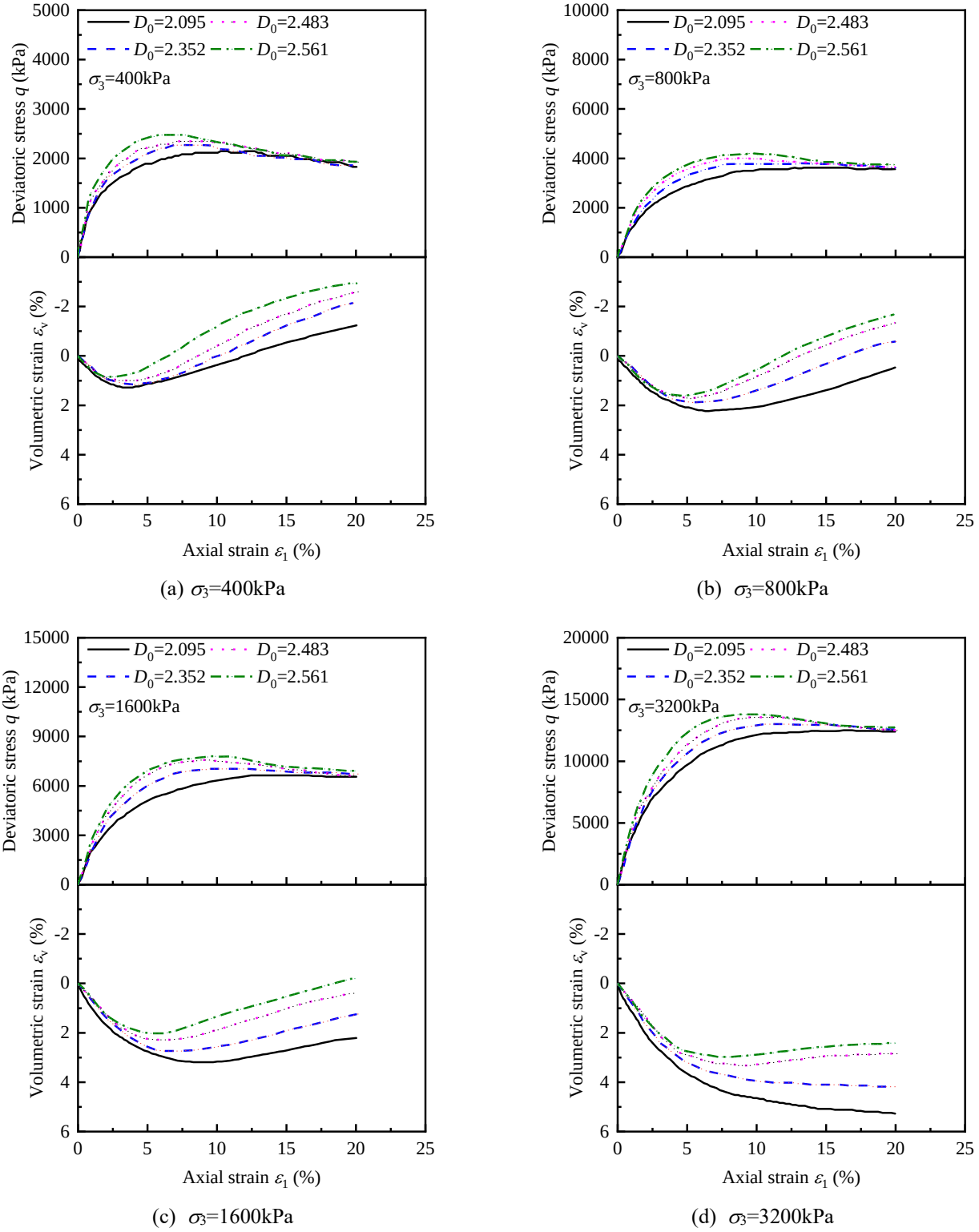

(a) σ_3=400kPa (b) σ_3=800kPa

(c) σ_3=1600kPa (d) σ_3=3200kPa

Fig. 5 Evolutions of deviatoric stress and volumetric strain with axial strain under different gradations

as shown in Fig. 7. By fitting and analyzing all the critical state points, it is found that they form a straight line passing through the origin, with a slope of approximately 1.72. This result indicates that there is no correlation between the critical state line and gradation, which is consistent with the findings of Li *et al.* (2015). This straight line is defined as the CSL in the q-p' plane, and its slope represents the critical stress ratio, which can be expressed as

$$\eta_c = q_c / p'_c \tag{2}$$

Where η_c is the critical stress ratio, q_c is the critical

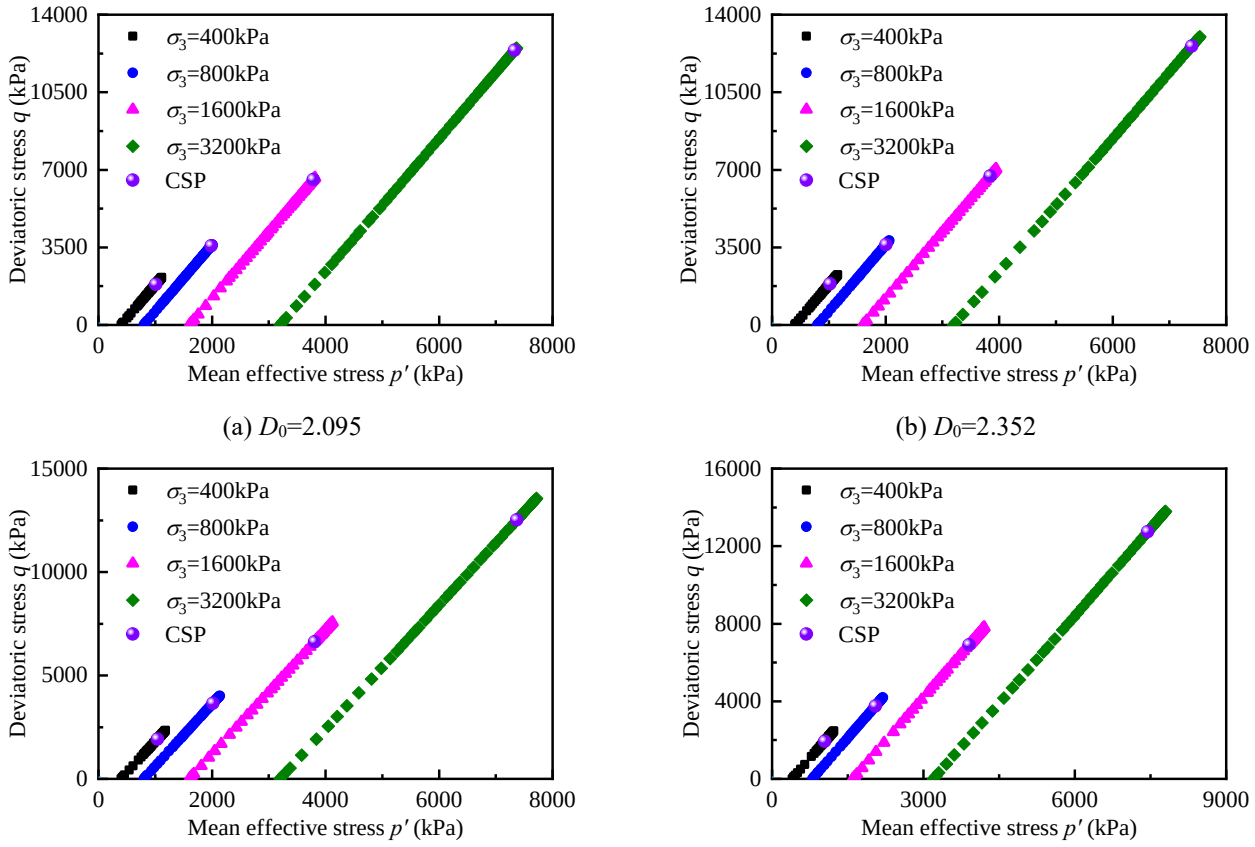

(a) D_0=2.095 (b) D_0=2.352

(c) D_0=2.483 (d) D_0=2.561

Fig. 6 Stress path and critical state point in the q-p' plane

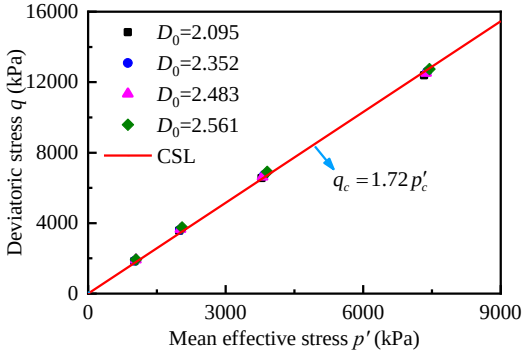

Fig. 7 CSL in the q-p' plane

deviatoric stress, and p'_c is the critical mean effective stress.

4.2 CSL in the e-(p′/pa)ξ plane

Fig. 8 shows the trend of changes in void ratio during the triaxial tests. It can be observed that under low confining pressure, the void ratio initially decreases with the increase of mean effective stress, reaches a minimum value, then begins to rise, and continues to increase after the mean effective stress reaches its peak, until it reaches the critical void ratio. This process reflects the behavior of dilation and strain softening. In contrast, under high confining pressure, the variation of void ratio follows a different pattern: when the fractal dimension is low, the void ratio decreases directly to the critical value as the confining pressure increases, indicating continuous volume contraction throughout the test. However, when the fractal dimension is high, the void ratio first decreases for a significant period, reaches the minimum value, and then increases slightly, which also reveals the sample's dilation behavior. As the fractal dimension increases, the tendency for dilation and strain softening becomes more pronounced.

The critical state points are summarized and plotted in the e-$(p'/p_a)^{\xi}$ plane, as shown in Fig. 9. It can be observed that as the fractal dimension increases, the CSL shifts downward, the intercept decreases, and the slope also becomes smaller. This is because changes in gradation cause the CSL to rotate, and similar results have also been reported by Xiao *et al.* (2023). This behavior is different from the variation of the CSL in the q-p' plane. In the e-$(p'/p_a)^{\xi}$ plane, the relationship between the void ratio and mean effective stress at critical state can be expressed as

$$e_c = e_\Gamma - \lambda_c \left(\frac{p}{p_a} \right)^{\xi} \tag{3}$$

Where e_c is the critical state void ratio, e_Γ is the critical void ratio when the mean effective stress is 0, λ_c is the slope

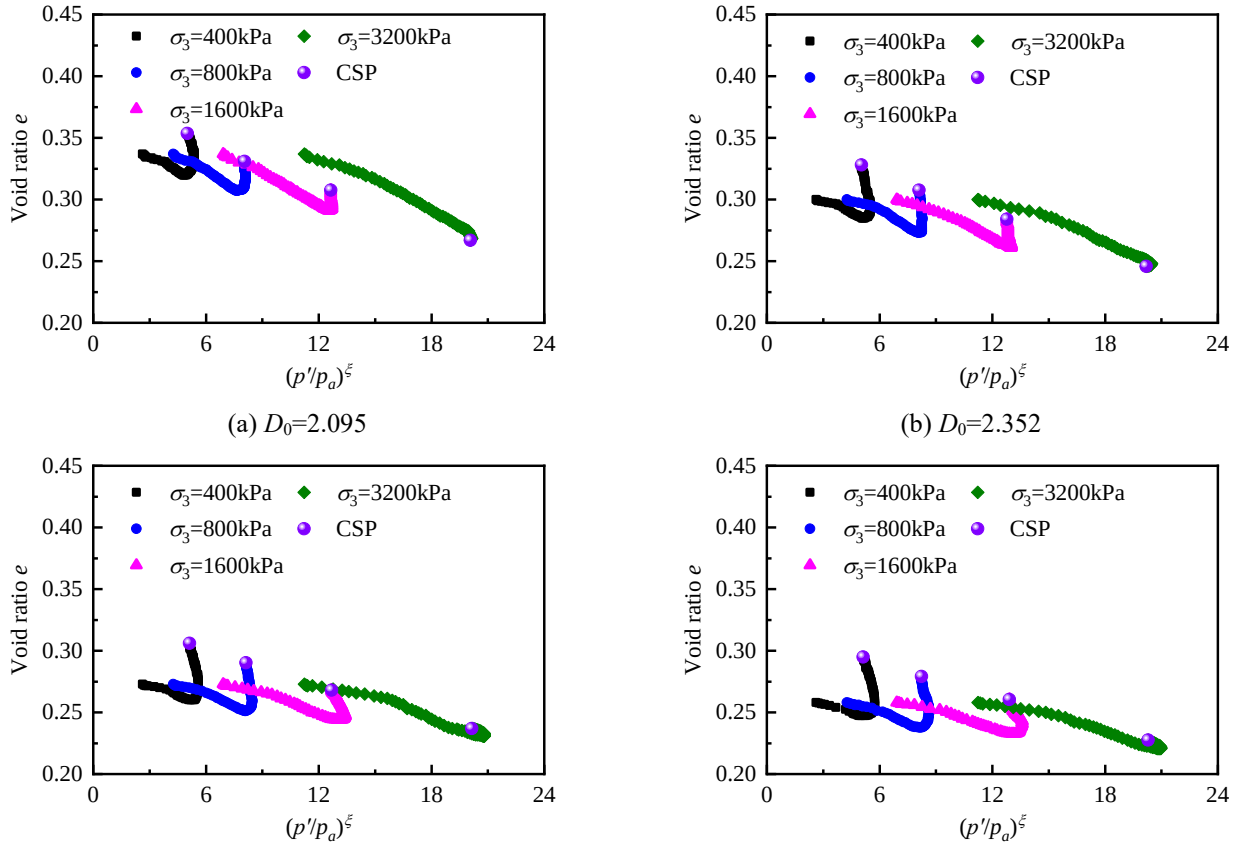

(a) D_0=2.095 (b) D_0=2.352

(c) D_0=2.483 (d) D_0=2.561

Fig. 8 Evolutions of void ratio in the e-$(p'/p_a)^{\xi}$ plane and critical state points

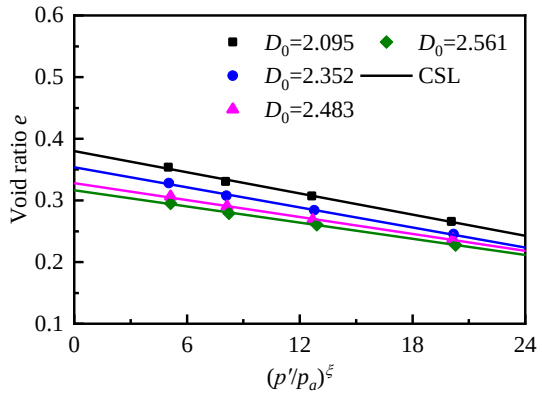

Fig. 9 CSL in the e-$(p'/p_a)^{\xi}$ plane

Table 2 Parameters of CSL in the e-$(p'/p_a)^{\xi}$ plane

Group	D_0	e_Γ	λ_c	ξ	R^2
G1	2.095	0.3801	0.0057	0.7	0.988
G2	2.352	0.3536	0.0054	0.7	0.995
G3	2.483	0.3278	0.0046	0.7	0.991
G4	2.561	0.3163	0.0044	0.7	0.999

of the CSL, ξ is the material parameter, and ξ typically takes value of 0.7. In this study, the values of e_Γ, λ_c and ξ are listed in Table 2.

In summary, the initial gradation of the sample has little effect on the CSL in the q-p' plane, meaning the critical stress ratio remains a constant. However, upon reanalyzing the definition of critical state, it becomes clear that the CSL in the q-p' plane only provides information about shear stress and mean effective stress, while neglecting the important factor of volume strain. Therefore, the unique CSL in the q-p' plane alone cannot determine that gradation has no effect on the critical state.

By combining the CSL in the e-$(p'/p_a)^{\xi}$ plane, it can be observed that gradation causes the CSL to shift downward and to the left, accompanied by some rotation, indicating that the critical void ratio is influenced by gradation. Therefore, it can be concluded that gradation has no effects on the critical stress ratio but significantly influences the critical void ratio.

5. A unique CSL by considering the skeleton void ratio

5.1 Review of skeleton void ratio

Granular materials, when compacted, inevitably form a skeleton of force chains and voids. However, in addition to the skeleton particles and voids, there exist fine particles within the voids between larger particles that do not

participate in force chain transmission. Some researchers (Yang *et al*. 2015, Dai *et al*. 2019, Wang *et al*. 2022) have debated whether these fine particles, which do not transmit forces, should be considered as part of the soil in the calculation of the void ratio. Thevanayagam (2007) considered the space occupied by fine particles, which do not contribute to the skeleton, as voids, and introduced the concept of the skeleton void ratio, which better reflects the true density.

Georgiannou *et al*. (1990) proposed an expression for the skeleton void ratio for clay-sand mixtures, where all fine particles are considered as voids

$$e_{sk} = \frac{V_v - V_f}{V_c} \tag{4}$$

Where V_v is void volume, V_f is volume of fine particles, and V_c is volume of coarse particles.

Using a packing model for sand–silt mixtures, Chang and Yin (2011) derived the skeleton void ratio for gravel-dominated gravelly sand as follows

$$e_{sk} = \frac{e-(a-1)Fc}{1-Fc} \tag{5}$$

where a is a material constant that represents the extent to which sand grains disrupt the gravel grain skeleton.

The above expression for the skeleton void ratio treats all fine particles as voids. However, not all fine particles do not contribute to the skeleton structure; some fine particles may have a potential passive role in force transmission (Wang *et al*. 2022). Therefore, fine particles that contribute to the skeleton structure should not be considered as voids. To provide a clear definition of the skeleton void ratio, Thevanayagam *et al*. (2002, 2007) conducted systematic research and classified skeleton structures under different fine particle contents. They defined a threshold for fine particle content, Fc_{th}, and divided the skeleton structure into two main categories: (1) when the fine particle content is below this threshold, the skeleton structure is dominated by coarse particles; (2) when the fine particle content exceeds this threshold, the skeleton structure is dominated by fine particles. Furthermore, each main category of the skeleton structure can be further divided into two subcategories based on the contact state of the internal particles, resulting in a total of four types of skeleton structures, as shown in Fig. 10.

In Fig. 10, b is the proportion of fine particles that participate in the force transmission among all fine particles, and Fc is the proportion of fine particles in the sample. The parameter b ranges from 0 to 1, where b=0 indicates that none of the fine particles participate in force transmission (state 1), and b=1 indicates that all fine particles actively participate in force transmission (where the skeleton void ratio e_{sk} degenerates to global void ratio e). Typically, particles with a diameter smaller than 5 mm are considered fine particles, and those with a diameter larger than 5 mm are considered coarse particles.

The parameter Fc can be calculated from the current gradation of the sample. However, the parameter b is difficult to obtain through laboratory tests, which greatly limits the promotion and application of the skeleton void ratio. Some researchers assume that b is independent of the fine particle content and can be given a fixed value. For instance, Thevanayagam and Martin (2002), in their study of sand-silt mixtures, used b=0.35. Clearly, this assumption is unreasonable. Rahman *et al*. (2011) argued that b should be a function of fine particle content and the ratio of coarse particle to fine particle diameters, and they developed an empirical formula for b as follows

$$\begin{cases} b = \left\{1-\exp\left[-0.3\dfrac{(Fc/Fc_{th})}{1-r^{0.25}}\right]\right\}\times\left(r\dfrac{Fc}{Fc_{th}}\right)^{r} \\ r = d_{50}/D_{10} \\ Fc_{th} = 0.4\left(\dfrac{1}{1+e^{\alpha-\beta r}}+r\right) \end{cases} \tag{6}$$

Where r is the particle size ratio of fine to coarse particles, d_{50} is the particle diameter corresponding to 50% of the fine particles, D_{10} is the particle diameter corresponding to 10% of the coarse particles, α and β are material constants.

Compared to the global void ratio, although the skeleton void ratio has advantages in representing the mechanical properties of granular soils, its practical application is still limited, primarily due to the difficulty in obtaining the parameter b value. In addition, no method for determining the b value suitable for coarse-grained soil has been proposed so far.

5.2 Establishment of a unique CSL equation

Different graded granular materials are essentially the same material. The critical state theory posits that there exists a unique CSL for the same material. To establish an equation that accurately reflects the CSL, the concept of the skeleton void ratio is introduced. The authors have constructed the following CSL equation

$$e_{csk} = e_{\Gamma sk} - \lambda_{csk}\left(\frac{p}{p_a}\right)^{\xi} \tag{7}$$

Where e_{csk} is the critical skeleton void ratio, $e_{\Gamma sk}$ is the critical skeleton void ratio when the mean effective stress is 0, λ_{csk} is the slope of CSL in the e_{sk}-$(p'/p_a)^{\xi}$ plane.

Based on the previous description of the skeleton void ratio, there are four types of skeleton structures. The skeleton structure suitable for coarse-grained soil is state 2, where the skeleton structure is predominantly composed of coarse particles, with some fine particles involved. Therefore, the formula for calculating the critical skeleton void ratio can be derived as

$$e_{csk} = \frac{e_c + (1-b)Fc}{1-(1-b)Fc} \tag{8}$$

The challenge of the skeleton void ratio lies in the accurate calculation of the percentage of fine particles involved in the force chain skeleton. Although the parameter b has clear physical meaning, it is difficult to obtain through laboratory tests. Currently, the most widely accepted semi-empirical formula was proposed by Rahman

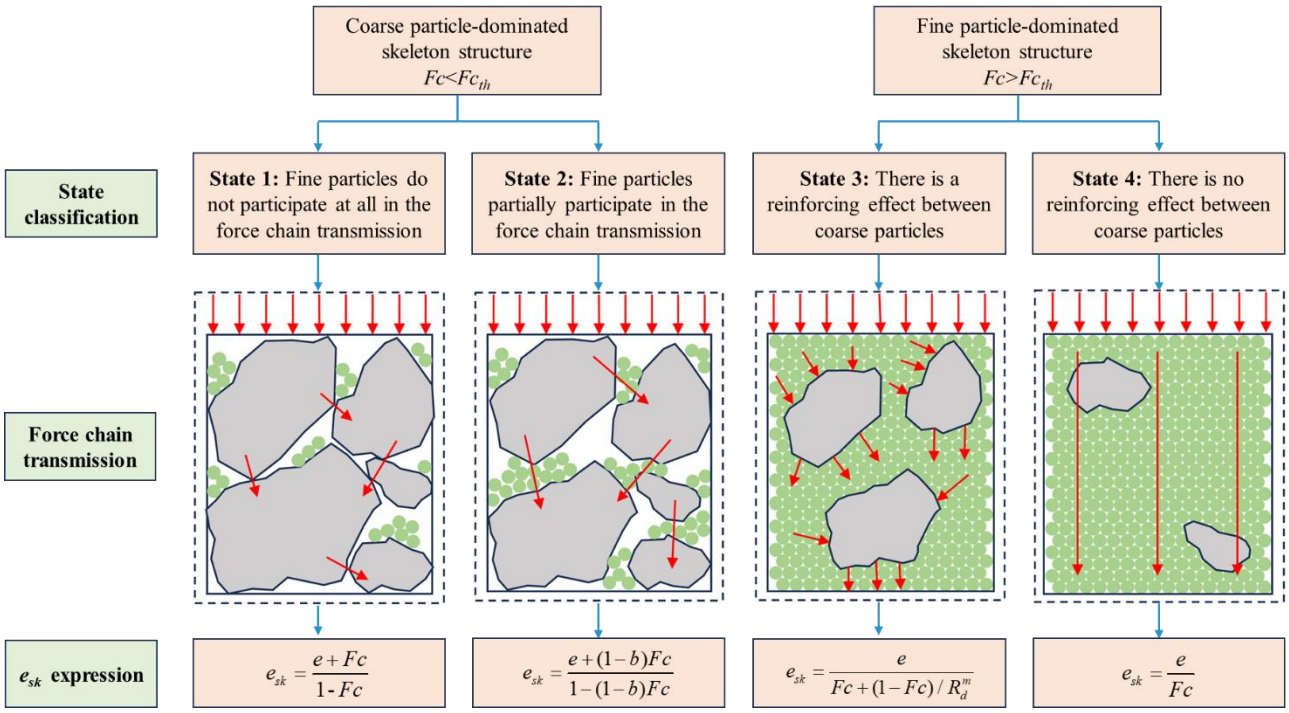

Fig. 10 Classification of skeleton structures and the expression of skeleton void ratio

Table 3 Values of the parameter *b*

Group	D_0	σ_3 (kPa)	*b* / %
G1	2.095	400	29.6
G1	2.095	800	36.1
G1	2.095	1600	40.3
G1	2.095	3200	43.0
G2	2.352	400	44.3
G2	2.352	800	47.0
G2	2.352	1600	48.7
G2	2.352	3200	50.5
G3	2.483	400	53.4
G3	2.483	800	54.8
G3	2.483	1600	55.8
G3	2.483	3200	56.3
G4	2.561	400	58.7
G4	2.561	800	59.3
G4	2.561	1600	59.7
G4	2.561	3200	60.0

et al. (2011, 2014), as shown in Eq. (6). In this study, α and β are taken as 0.13 and -1.5, respectively. The specific calculated values of parameter *b* are shown in Table 3.

Fig. 11 shows the CSL in the e_{sk}-$(p'/p_a)^{\xi}$ plane after correction using the skeleton void ratio. As can be seen from the figure, after correcting for the skeleton void ratio and accurately calculating parameter *b*, the critical points under different gradations and confining pressures lie on the same straight line, with a slope of -0.0049 and an intercept of 0.5557.

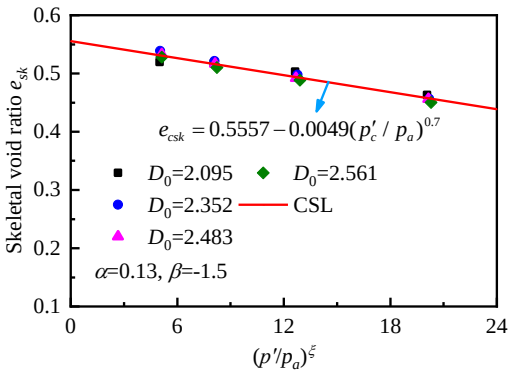

Fig. 11 CSL in the e_{sk}-$(p'/p_a)^{\xi}$ plane

From Eq. (6), it can be seen that the parameter *b* is a function of the particle size ratio of fine to coarse particles, the fine particle content, and the threshold fine particle content. In fact, all three factors are influenced by the gradation, which can be expressed through the fractal dimension. Therefore, it can be concluded that there is a certain mathematical relationship between the parameter *b* and the fractal dimension. Fig. 12 shows the relationship between parameter *b* and the fractal dimension under different initial gradations and confining pressures. It can be observed that there is a good linear relationship between *b* and the fractal dimension, which can be expressed as

$$b = mD + n \tag{9}$$

Where *m* and *n* are material constants.

5.3 Verification of the unique CSL equation

To verify the validity of Eq. (7), experimental data from

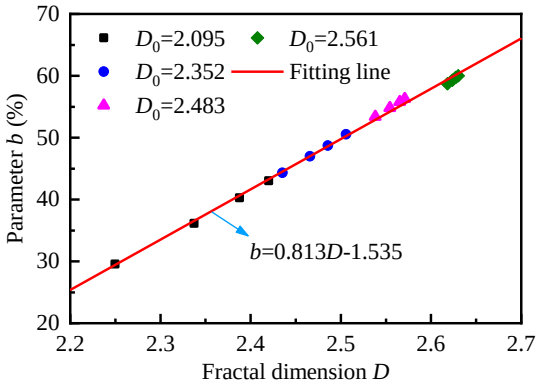

Fig. 12 Relationship between b and D

Xiao *et al*. (2023) are used for validation analysis. The initial gradations in the experiment had uniformity coefficients C_u of 5, 10, 20, and 40, corresponding to fractal dimensions of 1.879, 2.222, 2.397, and 2.511, respectively.

Fig. 13 shows the results before and after correction of the CSL using the skeleton void ratio, as well as the relationship between parameter b and the fractal dimension. It can be observed that in the e-$(p'/p_a)^{\xi}$ plane, as the uniformity coefficient increases, the CSL gradually shifts downward and also experiences some rotation. In the e_{sk}-$(p'/p_a)^{\xi}$ plane, the CSL of different initial gradations converge into a single straight line, consistent with the conclusions derived from the author's experiments, where the material parameters α and β were taken as 0.13 and -1.5, respectively. Furthermore, it is also observed that there exists a linear relationship between parameter b and fractal dimension, which further verifies the validity and applicability of the formula proposed in this study.

According to Eq. (9), there is a linear relationship between parameter b and fractal dimension D, indicating a one-to-one correspondence between them. Parameters b and D obtained from this study, as well as from Xiao *et al*. (2023), are plotted together on Fig. 14. It can be observed that the relationship between parameters b and fractal dimension D for the two datasets can be fitted with a single straight line with the same parameters value of m and n, further validating the rationality of Eq. (9).

5.4 Discussion on the applicability of Eq. (9)

Compared to Eq. (6), Eq. (9) significantly simplifies the calculation process for parameter b. However, the accuracy of Eq. (9) remains uncertain. Experimental data from Guo *et al*. (2024) were taken as an example. Fig. 15 presents a comparison of the b values calculated using Eqs. (6) and (9). In Eq. (9), the parameters m and n were set to 0.831 and -1.578, respectively, consistent with the experimental data from this study and Xiao *et al*. (2023), as shown in Fig. 14. It can be observed that the data points are distributed near a straight line passing through the origin with a slope of 1, indicating that for coarse-grained soil following a fractal distribution, Eq. (9) can serve as an approximate substitute for Eq. (6) with m=0.831 and n=-1.578.

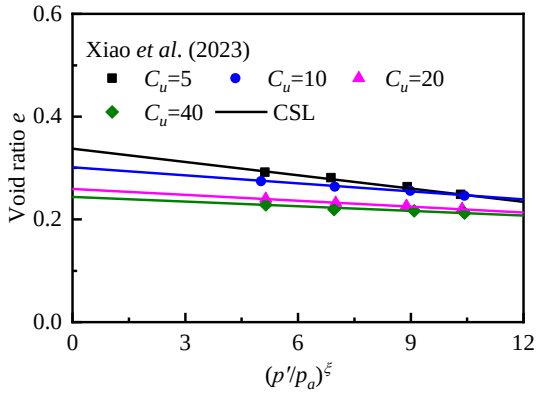

(a) e-$(p'/p_a)^{\xi}$ plane

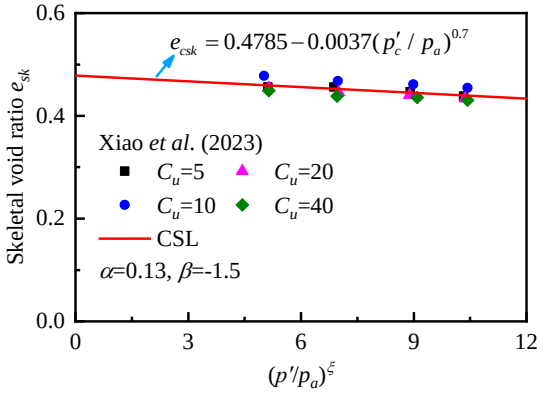

(b) e_{sk}-$(p'/p_a)^{\xi}$ plane

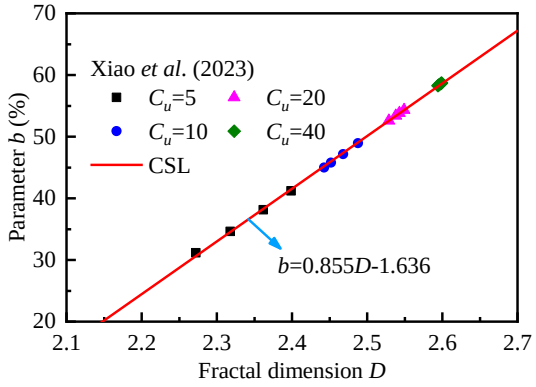

(c) Relationship between b and D

Fig. 13 Validation results using existing large-scale triaxial test data

Furthermore, substituting the parameter b calculated using Eq. (9) into Eq. (8) yields the critical state lines before and after the correction for skeleton void ratio, as shown in Fig. 16. These similar results to those of Xiao *et al*. (2023) were exhibited, further validating the applicability of the Eq. (9) and the unified CSL equation proposed.

The development of constitutive models for coarse-grained soils with different gradations currently requires distinct parameters, effectively treating soils with different gradations as different materials. This is primarily because the CSL parameters vary across different gradations, leading to different state parameters for the same stress-

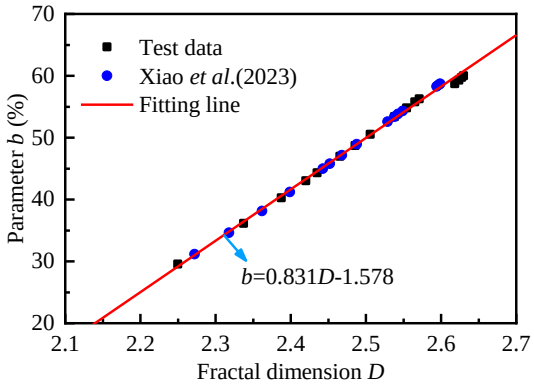

Fig. 14 Relationship between b and D with two data sources

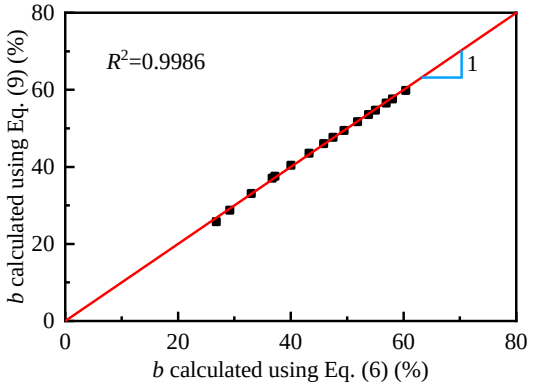

Fig. 15 Validation of the accuracy of b using Eq. (9)

strain condition, making it challenging to predict whether dilatancy or contraction will occur. The concept of the skeleton void ratio effectively addresses this critical issue, and its clear physical meaning has gained widespread recognition. However, the existing formula for calculating parameter b is overly complex, significantly hindering the adoption and application of the skeleton void ratio. The empirical linear relationship between parameter b and the fractal dimension proposed in this study simplifies the calculation process, providing a robust foundation for promoting and applying the skeleton void ratio.

Therefore, the findings of this study provide a method to determine the skeleton void ratio and a unified CSL across different gradations, thereby obtaining a unique state parameter. Based on the theoretical framework of state-dependent constitutive model (Li 2002), the obtained state parameter can be incorporated into the dilatancy equation, which is then integrated into the constitutive model, ultimately yielding a state-dependent constitutive model applicable to different gradations.

In addition, particle shape is recognized as another critical factor influencing the mechanical properties of granular materials (Payan *et al.* 2016a, Payan *et al.* 2019), such as the critical stress ratio (Payan *et al.* 2016b, Payan *et al.* 2017b). Typically, particle angularity increases the critical stress ratio by enhancing interparticle friction. However, it also promotes particle breakage, which in turn reduces the critical stress ratio. Therefore, the influence of particle angularity on the critical state behavior of coarse-grained soils is complex and warrants further investigation. Moreover, particle shape may indirectly affect the skeleton void ratio by modifying the force transmission network. For example, angular particles could increase the proportion of active fine particles participating in the skeleton, thereby reducing e_{sk}. However, quantitative studies on the influence of particle shape on the skeleton void ratio parameter b have not been reported. Therefore, future work should incorporate shape descriptors into Eq. (9) to further extend the applicability of the equation.

6. Conclusions

This study conducts triaxial compression tests on coarse-grained soils, to analyze the effects of confining pressure and initial gradation on CSLs of coarse-grained soils. The concept of skeleton void ratio is introduced, leading to a unified CSL equation for coarse-grained soils under different initial gradations. The CSL equation is then validated using experimental data and existing literature data. The main conclusions are as follows

- The influence of initial gradation on the CSL is primarily reflected in the volumetric strain. In the q-p' plane, the CSL does not change with variations in fractal dimension, remaining a straight line passing through the origin with a constant slope, indicating that the critical stress ratio is not affected by the initial gradation. However, in the e-$(p'/p_a)^{\xi}$ plane, as the fractal dimension increases, the CSL gradually shifts downward and rotates, indicating that the critical void ratio is influenced by the initial gradation.
- By replacing the global void ratio with the skeleton void ratio, a unified CSL can be obtained in the e_{sk}-$(p'/p_a)^{\xi}$ plane for different initial gradations. A major difficulty in developing state-dependent dilatancy equation is that the CSL is not unique for different initial gradations, making it challenging to predict whether the soil will exhibit dilatancy or contraction. The unified CSL equation proposed in this study provides a solid foundation for establishing state-dependent dilatancy equation and constitutive model for different gradations.
- There is a good linear relationship between the skeleton void ratio parameter b and the fractal dimension D. This finding facilitates the broader application of the skeleton void ratio. However, this linear relationship has only been validated for well-graded coarse-grained soils, and its applicability to discontinuous gradations or other granular materials, such as sand or carbonated sand, requires further investigation.

Acknowledgments

This work was supported by the National Natural Science Foundation of China (Grant No. 42407251), the

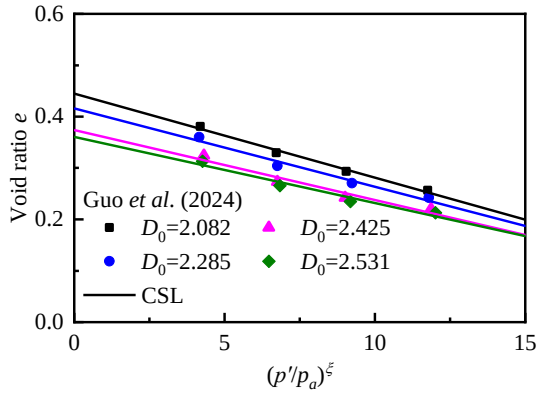

(a) In the e-$(p'/p_a)^{\xi}$ plane

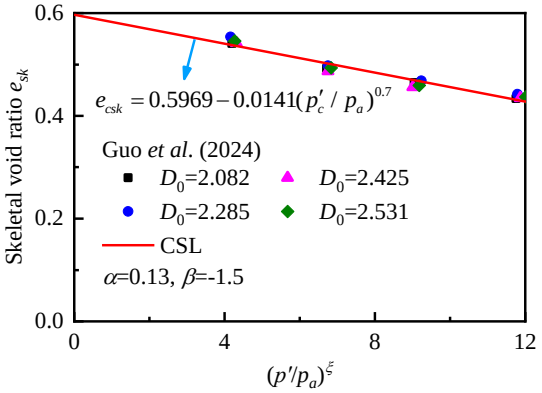

(b) Relationship between b and D

Fig. 16 Validation of the applicability of Eq. (9)

Scientific Project from Huaneng Company Headquarters (HNKJ20-H45), the Yangtze River Water Science Research Joint Fund (U2040221), and the Natural Science Foundation of Jiangsu Province (No. BK20230954).

References

Abadi, T., Madhusudhan, B.N., Li, H. and Le Pen, L. (2023), "Reusing life-expired railway ballast: Laboratory testing, shape analysis, and petrographic evaluation", *J. Geotech. Geoenviron. Eng.*, **149**(1), 04022123. https://doi.org/10.1061/(ASCE)GT.1943-5606.0002904.

Ahmed, S.S., Martinez, A. and DeJong, J.T. (2023), "Effect of gradation on the strength and stress-dilation behavior of coarse-grained soils in drained and undrained triaxial compression", *J. Geotech. Geoenviron. Eng.*, **149**(5), 04023019. https://doi.org/10.1061/JGGEFK.GTENG-10972.

ASTM D2487–06 (2006), Standard practice for classification of soils for engineering purposes (Unified Soil Classification System), American Society for Testing Materials; West Conshohocken, USA.

Baak, S.H., Cho, G.C. and Song, K.I. (2017), "Stability analysis on the concrete slab of the highest concrete-faced rock-fill dam in South Korea", *Geomech. Eng.*, **13**(5), 881-892. https://doi.org/10.12989/gae.2017.13.5.881.

Chang, C.S., Wang, J.Y. and Ge, L. (2015), "Modeling of minimum void ratio for sand-silt mixtures", *Eng. Geol.*, **196**, 293-304. https://doi.org/10.1016/j.enggeo.2015.07.015.

Chang, C.S. and Yin, Z.Y. (2011), "Micromechanical modeling for behavior of silty sand with influence of fine content", *Int. J. Solids. Struct.*, **48**(19), 2655-2667. https://doi.org/10.1016/j.ijsolstr.2011.05.014.

Chang, J.F., Chu, X.H. and Xu, Y.J. (2014), "A softening hyperelastic model and simulation of the failure of granular materials", *Geomech. Eng.*, **7**(4), 335-353. https://doi.org/10.12989/gae.2014.7.4.335.

Dai, B.B., Yang, J., Gu, X.Q. and Zhang, W. (2019), "A numerical analysis of the equivalent skeleton void ratio for silty sand", *Geomech. Eng.*, **17**(1), 19-30. https://doi.org/10.12989/gae.2019.17.1.019.

Dash, H.K. and Sitharam, T.G. (2011), "Cyclic liquefaction and pore pressure response of sand-silt mixtures", *Geomech. Eng.*, **3**(2), 83-108. https://doi.org/10.12989/gae.2011.3.2.083.

Fonseca, A.V.D., Molina-Gomez, F., Ferreira, C. and Quintero, J. (2023), "Modelling the critical state behaviour of granular soils: Application of NorSand constitutive law to TP-Lisbon sand", *Geomech. Eng.*, **34**(3), 317-328. https://doi.org/10.12989/gae.2023.34.3.317.

Georgiannou, V.N., Burland, J.B. and Hight, D.W. (1990), "The undrained behavior of clayey sands in triaxial compression and extension", *Géotechnique*, **40**(3), 431–449. https://doi.org/10.1680/geot.1990.40.3.431.

Guo, W.L., Song, D.Q. and Li, X.M. (2024), "Unified model of critical state line for rockfill material with and without considering particle breakage", *Acta. Geotech.*, **19**, 2273–2291. https://doi.org/10.1007/s11440-023-02095-w.

Jiang, M.D., Yang, Z.X., Barreto, D. and Xie, Y.H. (2018), "The influence of particle-size distribution on critical state behavior of spherical and non-spherical particle assemblies", *Granul. Matter.*, **20**, 80. https://doi.org/10.1007/s10035-018-0850-x.

Khodkari, N., Hamidian, P., Khodkari, H., Payan, M. and Behnood, A. (2024), "Predicting the small strain shear modulus of sands and sand-fines binary mixtures using machine learning algorithms", *Transp. Geotech.*, **44**, 101172. https://doi.org/10.1016/j.trgeo.2023.101172.

Kian, A.R.T., Zakeri, J.A. and Sadeghi, J. (2018), "Experimental investigation of effects of sand contamination on strain modulus of railway ballast", *Geomech. Eng.*, **14**(6), 563-570. https://doi.org/10.12989/gae.2018.14.6.563.

Li, G., Liu, Y.J., Dano, C. and Hicher, P.Y. (2015), "Grading-dependent behavior of granular materials: from discrete to continuous modeling", *J. Eng. Mech.*, **141**(6), 04014172. https://doi.org/10.1061/(ASCE)EM.1943-7889.0000866.

Li, X.S. (2002), "A sand model with state-dependent dilatancy", *Géotechnique.*, **52**(3), 173-186. https://doi.org/10.1680/geot.2002.52.3.173.

Muir Wood, D. and Maeda, K. (2008), "Changing grading of soil: effect on critical states", *Acta. Geotech.*, **3**(1), 3-14. https://doi.org/10.1007/s11440-007-0041-0.

Ng, C.W.W., Zhang, Q., Zhang, S., Lau, S.Y., Guo, H. and Li, Z. (2024), "A new state-dependent constitutive model for cyclic thermo-mechanical behaviour of unsaturated vegetated soil", *Can. Geotech. J.*, **61**(10), 2155-2179. https://doi.org/10.1139/cgj-2023-0268.

Ning, F.W., Liu, J.M., Kong, X.J. and Zou, D.G. (2020), "Critical state and grading evolution of rockfill material under different triaxial compression tests", *Int. J. Geomech.*, **20**(2), 04019154. https://doi.org/10.1061/(asce)gm.1943-5622.0001550.

Payan, M., Senetakis, K. and Khalili, N. (2016a), "Influence of particle shape on small-strain damping ratio of dry sands", *Géotechnique.*, **66**(7), 610-616. https://doi.org/10.1680/jgeot.15.T.035.

Payan, M., Khoshghalb, A., Senetakis, K. and Khalili, N. (2016b), "Effect of particle shape and validity of G_{max} models for sand: A critical review and a new expression", *Comput. Geotech.*, **72**, 28-41. https://doi.org/10.1016/j.compgeo.2015.11.003.

Payan, M., Senetakis, K., Khoshghalb, A. and Khalili, N. (2017a), "Characterization of the small-strain dynamic behaviour of silty sands; contribution of silica non-plastic fines content", *Soil. Dyn. Earthq. Eng.*, **102**, 232-240. https://doi.org/10.1016/j.soildyn.2017.08.008.

Payan, M., Senetakis, K., Khoshghalb, A. and Khalili, N. (2017b), "Effect of gradation and particle shape on small-strain Young's modulus and Poisson's ratio of sands", *Int. J. Geomech.*, **17**(5), 04016120. https://doi.org/10.1061/(asce)gm.1943-5622.0000811.

Payan, M. and Senetakis, K. (2018), "Effect of anisotropic stress state on elastic shear stiffness of sand–silt mixture", *Geotech. Geol. Eng.*, **37** (3), 2237-2244. https://doi.org/10.1007/s10706-018-0690-9.

Payan, M. and Chenari, R.J. (2019), "Small strain shear modulus of anisotropically loaded sands", *Soil. Dyn. Earthq. Eng.*, **125**, 105726. https://doi.org/10.1016/j.soildyn.2019.105726.

Payan, M., Khoshini, M. and Chenari, R.J. (2020), "Elastic dynamic Young's modulus and Poisson's ratio of sand–silt mixtures", *J. Mater. Civ. Eng.*, **32** (1), 04019314. https://doi.org/10.1061/(asce)mt.1943-5533.0002991.

Rahman, M.M., Lo, S.C.R. and Dafalias, Y.F. (2014), "Modelling the static liquefaction of sand with low-plasticity fines", *Géotechnique*, **64**(11), 881-894. https://doi.org/10.1680/geot.14.P.079.

Rahman, M.M., Lo, S.R. and Baki, M.A.L. (2011), "Equivalent granular state parameter and undrained behaviour of sand-fines mixtures", *Acta. Geotech.*, **6**(4), 183-194. https://doi.org/10.1007/s11440-011-0145-4.

Shi, J.W., Chen, Y.H., Kong, G.Q., Lu, H., Chen, G. and Shi, C. (2024), "Deformation mechanisms of an existing pipeline due to progressively passive instability of tunnel face: Physical and numerical investigations", *Tunn. Undergr. Sp. Tech.*, **150**, 105822. https://doi.org/10.1016/j.tust.2024.105822.

Shi, J.W., Zhong, X.C., Lu, H., Ni, X.D. and Shi, C. (2025), "Influence of joint stiffness on three-dimensional deformation mechanisms of pipeline under tunnel active face instability", *Can. Geotech. J.*, **62**, 1-16. https://doi.org/10.1139/cgj-2024-0092.

Sun, Y.F., Wang, Z.T. and Gao, Y.F. (2019), "Mechanistic representation of the grading-dependent aggregates resiliency using stress transmission column", *Geomech. Eng.*, **17**(4), 405-411. https://doi.org/10.12989/gae.2019.17.4.405.

Thevanayagam, S. (2007), "Intergrain contact density indices for granular mixes - I: Framework", *Earthq. Eng. Eng. Vib.*, **6**(2), 123-134. https://doi.org/10.1007/s11803-007-0705-7.

Thevanayagam, S. and Martin, G.R. (2002), "Liquefaction in silty soils - screening and remediation issues", *Soil. Dyn. Earthq. Eng.*, **22**(9-12), 1035-1042. https://doi.org/10.1016/S0267-7261(02)00128-8.

Wang, T., Liu, S.H., Wautier, A. and Nicot, F. (2022), "Updated skeleton void ratio for gravelly sand mixtures considering effect of grain-size distribution", *Can. Geotech. J.*, **59**(1), 12-23. https://doi.org/10.1139/cgj-2020-0570.

Wu, E.L., Zhu, J.G., Wang, J.J., Guo, W.L., Wang, L. and Wang, W. (2024), "Investigation on the incremental creep model of rockfill material for dam building", *Comput. Geotech.*, **174**, 106636. https://doi.org/10.1016/j.compgeo.2024.106636.

Xiao, Y., Liu, H.L., Ding, X.M., Chen, Y.M., Jiang, J.S. and Zhang, W.G. (2016), "Influence of particle breakage on critical state line of rockfill material", *Int. J. Geomech.*, **16**(1), 04015031. https://doi.org/10.1061/(asce)gm.1943-5622.0000538.

Xiao, Y., Meng, M.Q., Wang, C.G., Wu, H.R., Fang, Q.Y. and Liu, S. (2023), "Breakage critical state of gravels with different gradings. Part I: Experimental results", *Transp. Geotech.*, **42**, 101087. https://doi.org/10.1016/j.trgeo.2023.101087.

Yan, W.M. and Dong, J.J. (2011), "Effect of particle grading on the response of an idealized granular assemblage", *Int. J. Geomech.*, **11**(4), 276-285. https://doi.org/10.1061/(Asce)Gm.1943-5622.0000085.

Yang, J., Wei, L.M. and Dai, B.B. (2015), "State variables for silty sands: Global void ratio or skeleton void ratio?", *Soils. Found.*, **55**(1), 99-111. https://doi.org/10.1016/j.sandf.2014.12.008.

Yang, S.L., Sandven, R. and Grande, L. (2006), "Steady-state lines of sand-silt mixtures", *Can. Geotech. J.*, **43**(11), 1213-1219. https://doi.org/10.1139/T06-069.

Yin, Z.Y., Zhao, J.D. and Hicher, P.Y. (2014), "A micromechanics-based model for sand-silt mixtures", *Int. J. Solids. Struct.*, **51**(6), 1350-1363. https://doi.org/10.1016/j.ijsolstr.2013.12.027.

Zamani, A. and Montoya, B.M. (2018), "Undrained monotonic shear response of MICP-treated silty sands", *J. Geotech. Geoenviron. Eng.*, **144**(6), 04018029. https://doi.org/10.1061/(Asce)Gt.1943-5606.0001861.

GC